Korean J. Chem. Eng., 40(11), 2778-2786 (2023)
DOI: 10.1007/s11814-023-1530-z

pISSN: 0256-1115
eISSN: 1975-7220

Preparation of biomass-based yam solar absorber for enhanced solar evaporation application

Li Ting*, Jia Juan,†, Wang Yanqing*, Sun Hanxue*, Li Jiyan*, Zhu Zhaoqi*, and Liang Weidong*,†**

*College of Petrochemical Engineering, Lanzhou University of Technology,
Langongping Road 287, Lanzhou 730050, P. R. China
**CALB Co. Ltd., Changzhou, Jiangsu, China, 213000
(*Received 7 April 2023 • Revised 17 June 2023 • Accepted 10 July 2023*)

Abstract−The solar evaporation system has become a research hotspot in the field of photothermal conversion technology in recent years because of its high photothermal conversion efficiency and practicality of promotion. Biomass solar absorbers have excellent solar absorption properties and high solar-water vapor conversion, but they have the limitations of long feedstock production cycle and high carbonization temperature. As a kind of biomass materials, yam is not only inexpensive, but also has a short production cycle and rich pore structures. Therefore, in this paper, a yam based solar absorber with rich pore structure was prepared, and the photothermal conversion efficiency of the absorber was further investigated. The yam was treated with freeze-dried method and carbonized at different temperatures to obtain yam solar absorbers. Then the thermal stability and porosity of solar absorber was found to gradually rise as the treatment temperature increased. The solar absorption rate of the carbonized yam was close to 90% in the near UV-visible region. Solar-water vapor control experiments with different treatments of the solar absorber of the yam were carried out in simulated solar-driven interface steam generation system (SISGS). An absorber treated at 200 °C in the sun was found to have the best performance with a solar-water vapor conversion of about 90% and a water evaporation rate of 1.3164 kg m^{-2} h^{-1}.

Keywords: Solar Steam Generation, Conversation Efficiency, Biomass Solar Absorber

INTRODUCTION

Rapid population growth and economic development increasingly deplete the freshwater resources available on earth. Solar energy, as the most abundant, pollution-free and renewable energy in nature, is now attracting widespread attention for freshwater production [1-9]. To ensure the security of fresh water, a solar-driven interfacial vaporization desalination method is proposed herein to convert the solar energy absorbed by photothermal materials into thermal energy fit for local heating of water molecules at the gas-liquid interface to produce vapor [10-19]. Then, it is condensed to produce fresh water. And this method is considered as one of the most promising photo-thermal technologies for its high conversion efficiency and extensive application in seawater desalination, wastewater purification, sterilization, and liquid-liquid phase separation [20]. Therefore, it is particularly important to develop an ideal absorber characterized by broadband solar energy absorption, excellent solar thermal conversion performance, low thermal conductivity, high hydrophilicity, and the abundance of porous channels, which is convenient for alleviating the current scarcity of freshwater resources.

In recent years, there has been a growing interest in use of biomass-based materials as independent solar absorbers [21-23]. Attributed to its abundance in nature, high hydrophilicity, low cost and environmental friendliness, it performs well in solar interfacial vapor production. In the systems of solar-driven interfacial vaporization, the photothermal material is either set directly on the water surface or indirectly in contact with the overall water through restricted water channels [24-28]. Despite many efforts made to improve the efficiency of solar thermal conversion, it remains challenging to derive efficient and low-cost solar thermal materials from the readily available raw materials. Geng et al. [23] developed a novel low-cost system based on a common biowaste, pomelo peels (PPs) and fractal carbonized pomelo peels (FCPP), to achieve 98% solar spectral absorption, 1.95 kg m^{-2} h^{-1} evaporation rate, and 92.4% solar thermal efficiency. Jia et al. [29] derived a new bilayer photothermal material of alabaster/polyacrylamide composite (APAC) from alabaster, with the efficiency of solar-water vapor conversion reaching 85% at 1 sun illumination. Yang et al. [30] prepared a novel solar interfacial evaporation device by depositing polydopamine (PDA) and silver nanoparticles (Ag-NPs) on natural wood. The device reached a high evaporation rate of 1.58 kg m^{-2} h^{-1} under one sun (1 kW m^{-2}), while the evaporation efficiency reached 88.6%. Despite the excellent solar absorption properties and high solar-water vapor conversion efficiency, biomass solar absorbers still face the problems of long feedstock production cycle [33] and high carbonization temperature [32,35].

In this paper, yam solar absorbers were obtained from commercially available yams and then treated in air. After the characterization of its morphology, starch crystalline form and other properties by scanning electron microscopy and X-ray diffraction, it is found

†To whom correspondence should be addressed.
E-mail: 1635391909@qq.com, wdliangh@lut.edu.cn

that yam possesses a pore-like structure and hydrophilicity. The simple method used to prepare yam solar absorber, the short production cycle, the wide source of raw materials and excellent solar-water vapor conversion efficiency provide a new solution for the study of biomass solar absorber.

EXPERIMENTAL

1. Materials and Apparatus

Yams were purchased from supermarkets. Polyvinyl alcohol was purchased from Tianjin Guang fu Fine Chemical Research Institute. Graphite powder.

Main experimental apparatus: Electronic analytical balance (JJ124BC), Vacuum freeze dryer (FD-1A-50), Scanning electron microscope (JSM-6701F), Transmission electron microscope (JEOL-2010), X-ray electron diffractometer (D/Max-2400), Thermogravimetric analyzer (TGA/DSCI), Fourier transform infrared spectroscopy (FTIR-850), Flash method thermal conductivity analyzer (LFA447), Specific surface area analyzer (SXL-1002), Contact angle tester (DSA100), Xenon lamp solar source (CEL-S500/350).

2. Methods

2-1. Preparation of Yam Solar Absorbers

Yams purchased from supermarkets were cut into columns of 0.5 cm thickness and soaked in distilled water for two days, with water changes every 2 h during this period. Afterwards, the soaked yams were freeze-dried by using freezer dryer after pre-freezing at −18 °C for 8 h.

2-2. Treatment of Yam Solar Absorbers

The above-mentioned yams were placed in a muffle furnace and carbonized at 200 °C, 250 °C, 260 °C and 270 °C degrees for 2 h to investigate the effects of different carbonizing temperatures on their properties. The preparation steps are shown in Fig. 1.

The figure shows that the yam was freeze-dried with a very low density, which allowed it to be placed on the top of the dandelion without destroying the white crown hairs knotted into a pompom. This feature provides conditions for it to float freely at the interface of the water column.

To investigate the effect of different treatments on the solar-water evaporation rate of the solar absorber of the yam, this paper also used a flame to treat them [34] and prepare bilayer the solar absorber of the yam. Meanwhile, bilayer yam-graphite powder solar absorbers were prepared by coating the yam surface with PVA (10% concentration) followed by adhesion with graphite powder [36].

RESULTS AND DISCUSSION

SEM was used to determine the morphological characteristics of freeze-dried yam. Fig. 2(a), (b), and (c) are SEM images of freeze-dried yam treated at temperatures of 200 °C and 270 °C. A honeycomb-like structure can be seen on the yam's longitudinal surface, which is also filled with many granules that are both densely packed and sparsely distributed in different places. From Fig. 2(a) to (c), the damage to the structure increases as the temperature rises. To further validate this conclusion, the particle-filled regions were scaled up independently at various temperatures (Fig. 3).

Fig. 3(a) depicts the electron microscope scan of the freeze-dried yam in the granule-filled region, which shows that the skeleton of yam is intact and the granules are clustered within the skeleton. The picture captured by a scanning electron microscope of yam treated at 200 °C is depicted in Fig. 3(b). The skeleton in the illustration looks to be cracked, and although the stacked granules are still stacked, their stacked structure is beginning to disintegrate. Fig. 3(c) is a scanning electron microscopy image of yam following treatment at 270 °C, in which the skeleton was badly destroyed and particle accumulation was no longer compact. Therefore, when the temperature rises, so does the degree of skeletal structure damage. To have a deeper understanding of the yam's morphology, the cross-

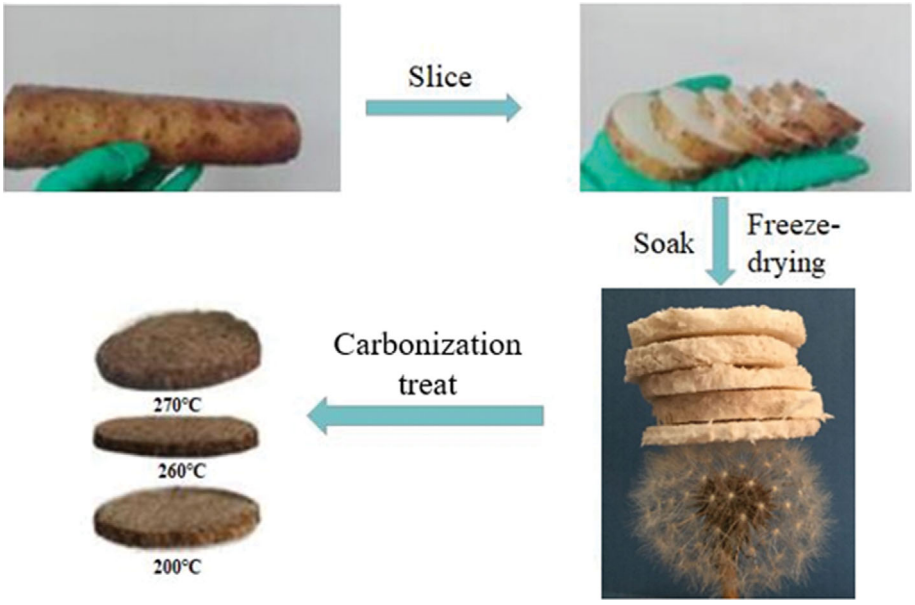

Fig. 1. The preparation process of the solar absorber of yam.

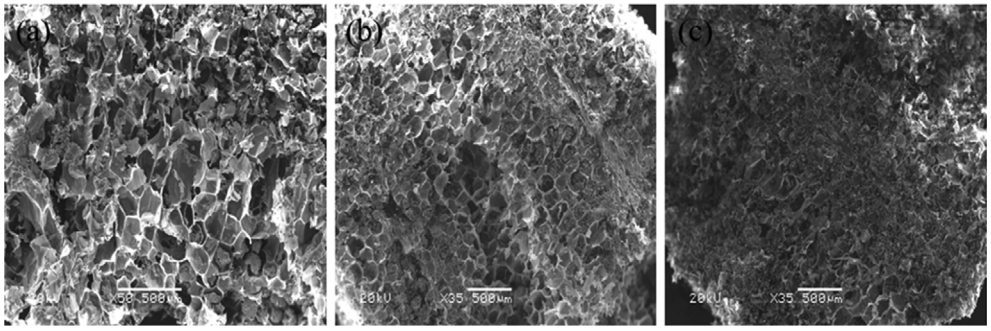

Fig. 2. SEM of the longitudinal section of yam; (a) yam after freeze-drying; (b) and (c) show the SEM of yam after carbonization at 200 °C and 270 °C, respectively.

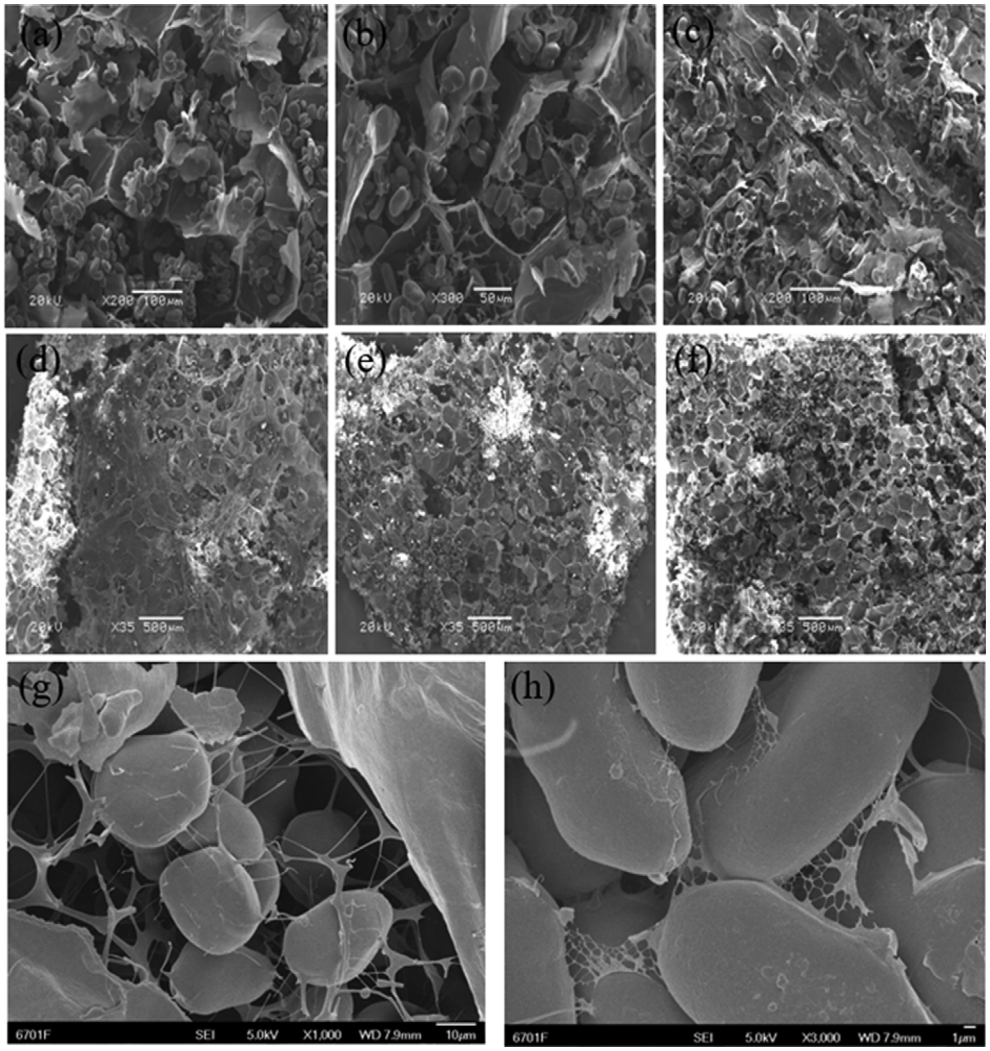

Fig. 3. SEM of yam in the area filled with particles; (a) yam after freeze-drying; (b) and (c) show the SEM of yam after carbonization at 200 °C and 270 °C, respectively. SEM of the Horizontal plane of yam; (d) yam after freeze-drying; (e) and (f) show the SEM of yam after carbonization at 200 °C and 270 °C, respectively; (g) SEM of the particle stack, (h) SEM of the skeleton wall.

section of the yam was described. As depicted, the particle accumulation zone and the particle sparse zone are evident, but the temperature damage to its structure becomes less apparent from Fig. 3(d) to (f), which may be related to the direction of its collapse. To further research the structure of the yam, the microscopic morphology of the granules and skeleton walls were examined. As illustrated in Fig. 3(g), the granules are connected to the skeleton and between the granules and the granules by a mesh structure, and the gran-

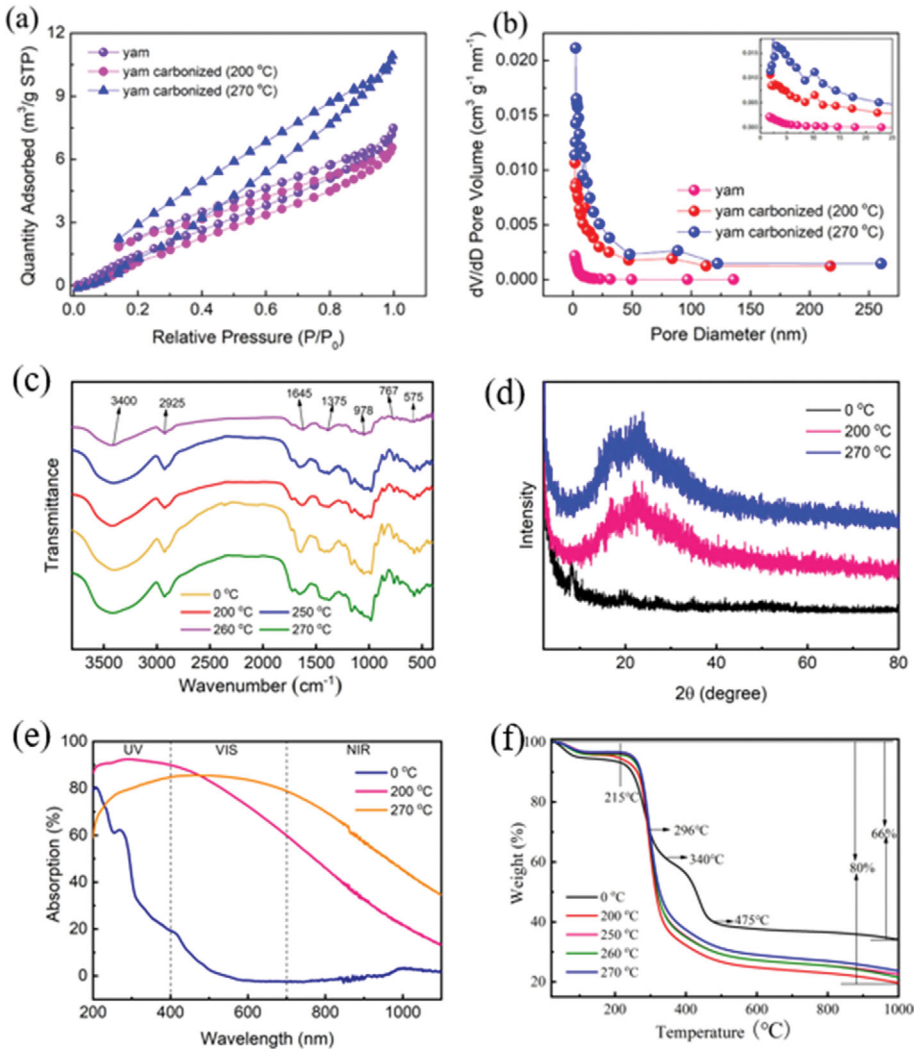

Fig. 4. (a) N_2-adsorption/desorption isotherms of the yam after being treated at different temperatures; (b) The pore size distribution of the yam after being treated at different temperatures; (c) FT-IR spectra of yam after being treated at different temperatures; (d) XRD patterns about yam after being treated at different temperatures; (e) The solar absorption of the solar absorber from 250 nm to 2,500 nm; (f) TGA graph of solar absorber.

ules have a smooth surface and a radius of approximately 10 μm. On the skeleton wall, as depicted in Fig. 3(h), there are folds and mesh-like branches, but no pore structure, and this unique structure can better sustain its particle structure.

The desorption curves of yam treated with different temperatures after freeze-drying were measured by the N_2 adsorption/desorption (77 K, P/P_0=0.975) method, and the average pore diameter and pore volume were obtained after calculation. The nitrogen adsorption and desorption isotherm curves and pore size distribution of yam are shown in Fig. 4(a) and (b). According to the International Union of Pure and Applied Chemistry (IUPAC) classification [35], the nitrogen adsorption and desorption isothermal curves in Fig. 4(a) are V-shaped, starting with microporous adsorption, and with the increase of pressure the capillary condensation phenomenon occurs to make the adsorption of the material rise rapidly; a hysteresis loop appears because capillary condensation and evaporation occur at different pressures. The pore size distribution of the material is shown by Fig. 4(b). It can be seen that the pore size distribution of the yam is wide and slightly different for the yam treated at different temperatures. In addition, the material pore diameters and adsorption pore volumes are shown in Table 1.

Table 1. Pore properties of solar absorber

Sample	V_{total} (cm^3 g^{-1})	D_{BJH} (nm)
Yam	0.010586	4.6960
Yam carbonized (200 °C)	0.056951	5.2257
Yam carbonized (270 °C)	0.009012	5.0569

Fig. 4(c) shows the chemical composition of the dried, the solar absorber of the yam, and the infrared absorption spectra of the solar absorbers in the range of 4,000-400 cm^{-1} were tested with the diffraction of the crystals to X-rays within 2-80°. In Fig. 4(c), the infrared absorption peaks near 3,400 cm^{-1} and 1,645 cm^{-1} are bending vibration absorption peaks of O-H chemical bonds [37]. The infra-

red absorption peak near 2,925 cm^{-1} is a stretching vibration absorption peak of -CH_2-. The IR absorption peaks near 1,645 cm^{-1} are the bending vibration absorption peaks of the O-H chemical bond [37] and possibly the C=O stretching vibration absorption peaks of the carbonyl group [38], and the absorption peaks at 1,375 cm^{-1}, 978 cm^{-1}, 765 cm^{-1} and 575 cm^{-1} are characteristic peaks of starch and glycosides [39]. Therefore, yam is rich in starch and sugar components [40], and the granules in its morphological analysis are starch, and hydrophilic groups such as O-H and C=O are the main reasons for the excellent hydrophilic properties of yam. By analysis, the main functional groups of yams treated at different temperatures did not undergo red shift or blue shift, but their fingerprint regions differed.

In the XRD patterns of Fig. 4(d), indicating two different peaks at 17° and 23°, we can find with increasing temperature, its crystallinity enhanced but its crystal type remained the same, and the diffraction peak at 23° indicated that the yam starch was a C-type crystal [41].

The spectral absorption curves of yam solar absorbers can be found in Fig. 4(e). From the figure, we can see that in the infrared and visible regions, the solar absorption by the treated the solar absorber of the yam is significantly higher than that before treatment, and the wavelengths corresponding to the maximum absorption of solar are different at different treatment temperatures The solar absorption weakens with the growth of wavelength in the near ultraviolet region, but in the visible region, its solar absorption can reach over 80%.

To investigate the effect of treatment temperature on the thermal stability properties of yam, the variation of mass with temperature was tested with a thermogravimetric analyzer under a nitrogen atmosphere at a heating rate of 10 °C/min, as shown in Fig. 4(f). From the figure, yams treated at different temperatures had the same rate of mass loss around 296 °C. Before this point, the mass loss of yams decreased with the increase of treatment temperature. After this point, the stability performance of the untreated yam was the best. Meanwhile, the untreated yam showed a plateau at 340 °C and then lost its quality again, and its quality was almost unchanged by 475 °C. For the treated yams, their thermal stability performance was enhanced with the increase of treatment temperature. During the temperature increase from room temperature to 1,000 °C, the yam lost 66% of mass for the untreated yam and 80% of mass for the 200 °C treatment; the yam lost very little mass until 215 °C, and the mass remained unchanged after 600 °C.

Solar absorbers efficiently utilize sun solar by containing the converted heat energy in the upper layer of the solar absorber, preventing heat loss into the water column. To determine this property of the solar absorber, the thermal conductivity of the laser method was used to measure the relevant data in this experiment. The thermal conductivity of a material can be calculated by the following equation:

Table 2. Thermal conductivity and related parameters

Samples	Thermal diffusivity ($mm^2\ s^{-1}$)	Specific heat ($J\ g^{-1}\ K^{-1}$)	Density ($g\ cm^{-3}$)	Thermal conductivity ($W\ m^{-1}\ K^{-1}$)
Yam				
Yam carbonized	0.09	1.751	1.267	0.201
(200 °C)	0.05	1.516	1.046	0.079

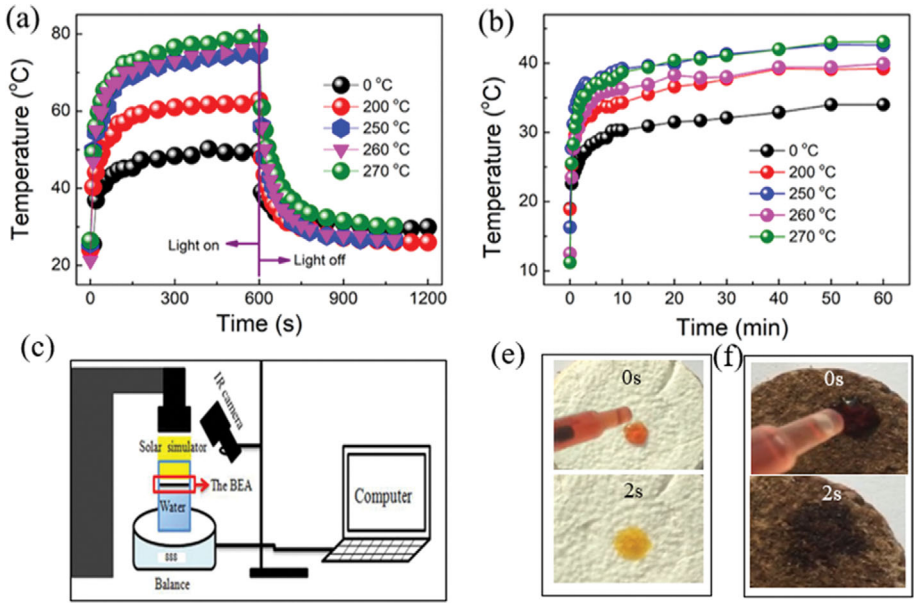

Fig. 5. (a) Surface temperature change of solar absorber in ai; (b) Surface temperature change of solar absorber in air on water; (c) Schematic of the solar-driven interfacial evaporation device; (d), (e) Photos of water droplets on solar absorber of yam.

$$K=\alpha C_p \rho$$

where K is the thermal diffusion coefficient and α is the thermal diffusivity. The thermal conductivity and related parameters are shown in Table 2. The thermal conductivity of the yam solar absorber is only 0.201 W/(m K), and the thermal conductivity is even lower at 0.079 W/(m K) after 200 °C treatment, so the treated yam is more favorable for SISGS to utilize solar energy efficiently.

Fig. 5(a) and (b) show the temperature variation of yam in air and water with different temperature treatments under 1 sun illumination with time, respectively. The first 10 min in Fig. 5(a) shows the variation of surface temperature of yam under solar 1 solar intensity with time, and after 2 min, the surface temperature approaches the equilibrium state almost no longer rises with the increase of time. When the solar simulator was turned off after 10 min, the surface temperature of the yam decreased rapidly, and the temperature approached room temperature after 3 min. Therefore, the surface of the yam solar absorber is highly dependent on the solar intensity, and the higher the treatment temperature, the higher the temperature at which it reaches equilibrium. Fig. 5(b) shows the time-temperature curves of yam solar absorbers floating in water under the same conditions. From the figure, the temperature on the yam surface reaches equilibrium after 10 min, and the highest is only 40 °C, which is lower than the temperature in air, which is related to the absorption of heat generated from yam by the water body; it can be tentatively determined that the absorption mass of yam can be applied in solar steam production technology.

The freeze-dried yam has the advantages of porosity, hydrophilicity, and good thermal stability, and has high solar absorption in the near-infrared-visible region after treatment. To investigate the vapor rate and solar-water vapor conversion rate of the solar absorber of the yam applied to solar-distillation technology, solar-water vapor experiments were conducted under laboratory conditions, as shown in Fig. 5(c).

To test the hydrophilicity of the solar absorber of the yam to water and water transport properties, an experiment was designed

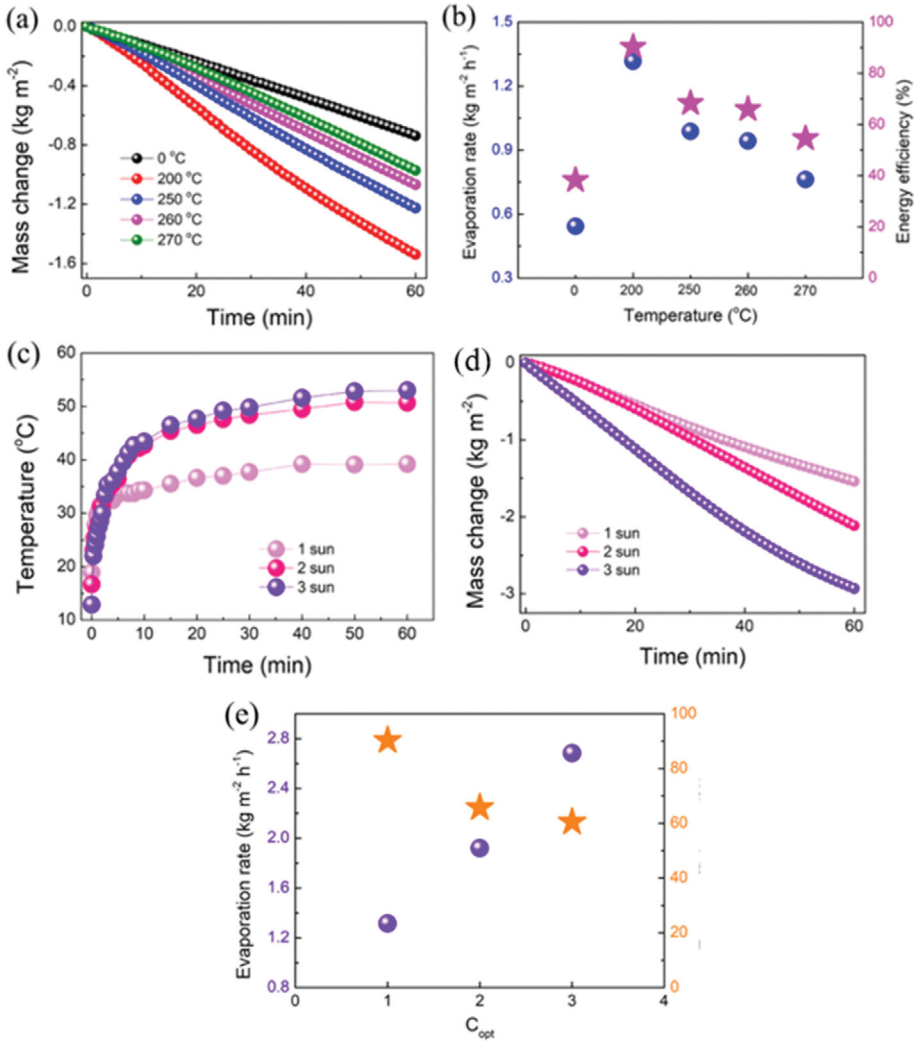

Fig. 6. (a) Time-dependent mass change of the yam under 1 illumination; (b) Evaporation rate (blue, left-hand side axis) and solar steam efficiency (pink, right-hand side axis) under 1 illumination; (c) Surface temperature change of the carbonized yam in 200 °C under different illumination; (d) Time-mass change of the carbonized yam in 200 °C under different illumination; (e) Evaporation rate (purple, left-hand side axis) and solar steam efficiency (yellow, right-hand side axis) under different illumination.

to drop water drops onto the surface of the solar absorbers with a syringe, as shown in Fig. 5(e) and (f). As can be seen in Fig. 5(e), the freeze-dried yam is hydrophilic, and the water droplets spread completely and transport some water below the interface after 2 s onto the surface of the solar absorber. From Fig. 5(f), we can see that the water droplets disappear after 2 s on the surface of the solar absorber, and the hydrophilicity of the solar absorber and the transport properties of the water body are improved after the surface treatment. This yam property may be related to the fact that yam itself has many hydrophilic groups, or it may be related to the structure of the pores after freeze-drying, or it may be caused by the interaction of both.

The curves of water mass loss with time due to yam absorbers after different temperature treatments under 1 sun illumination are shown in Fig. 6(a). From the figure, the treated yams caused greater mass loss in the water column than the untreated ones at the same time, and the 200 °C carbonized yams caused the greatest mass loss, which may be related to the changes in the structure of the yams during treatment. The amount of steam produced per unit time (steam rate) is calculated by deriving the mass change, and then the solar-water steam conversion efficiency is calculated by the following equation:

$$\eta = \dot{m} h_{LV} / C_{opt} q_i$$

where η is the solar photothermal conversion rate, $\dot{m}$ is the amount of water vapor production obtained, h_{LV} is the total enthalpy (including both latent and sensible heat), q_i is the value of solar radiation at 1 solar intensity, and $C_{opt}q_i$ is the total power density of solar irradiation. There are differences in the performance of solar absorbers at different optical densities [31,32], and in this paper 200 °C-carbonized yams were selected for solar water vapor experiments at different optical densities. Fig. 6(c) shows the variation of temperature with time at the interface with air when the yam is floating with the surface of the water body since different optical densities. As can be seen, the surface temperature of yam reached equilibrium after 10 min, less than 40 °C at 1-sun intensity, about 10 °C higher at 2-sun than at 1-sun, and the surface temperature of the solar absorber at 3-sun was similar to that at 2-sun, with no significant temperature increase. Fig. 6(d) shows the time-mass variation curves at different optical densities. It can be seen that the mass change under 3-sun optical density is greater than that under 1 and 2-sun. Comparing Fig. 6(c), the lowest yam surface temperature under 3-sun may be related to the fact that the heat produced by the yam is absorbed by the water body. Fig. 6(e) shows the evaporation rate of water vapor versus solar-water vapor conversion efficiency at different optical densities. As can be seen, the rate of water vapor production is proportional to the optical density, and the evaporation rate can reach 2.9 kg/(m^2 h) at 3 suns, but the solar-water vapor conversion efficiency decreases with increasing optical density. From 1 to 2 suns, the conversion rate decreases by about 25%, and from 2 to 3 suns its yield is close, decreasing by only about 5%.

To investigate the relationship between quality loss and the treatment of yam, experiments were designed for simple treatment of yam surface with flame and treatment of yam surface with PVA as adhesive and graphite powder as carbon material. It can be seen from Fig. 7(a) that the time required to reach the equilibrium temperature is close to the equilibrium temperature for the solar absorber of the yam treated with both methods. The change in mass per unit area with time, water vapor generation rate and solar-water

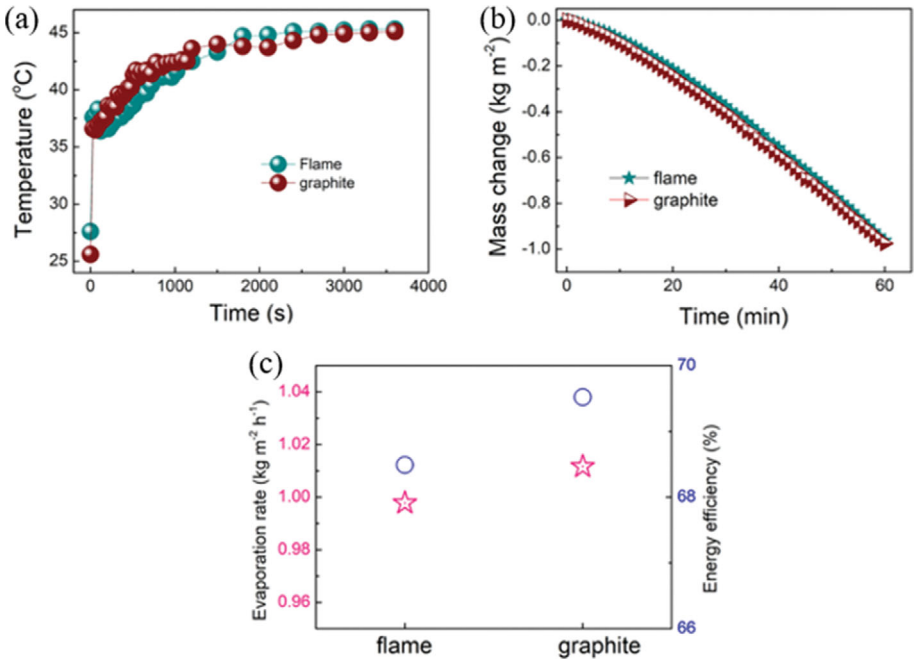

Fig. 7. (a) Surface temperature change of the yam treated by different carbon material under 1 illumination; (b) Time-dependent mass change of the yam treated by different carbon material under 1 illumination yam; (c) Evaporation rate (pink, left-hand side axis) and solar steam efficiency (blue, right-hand side axis) under 1 illumination.

vapor conversion rate for which graphite powder was the solar absorber layer were greater than that for yam treated with flame, and the solar-water vapor conversion rate for both was between 68-70%, which was lower than that for yam treated at 200 °C under the same conditions (about 90%). At the same time, the safety and the cheapness of raw materials of yam treated with 200 °C are higher than those treated with flame and with PVA and graphite powder, according to which, the 200 °C treatment of yam solar absorber has a better prospect in practical application.

CONCLUSIONS

Low-density yam solar absorbers were prepared from yam by freeze-drying and related treatments, and the solar-water vapor conversion efficiency of the solar absorbers was investigated. We found that freeze-dried yams with low thermal conductivity and macropores, mesoporous and microporous structures could absorb up to 90% of sunlight after treatment. The water vapor conversion efficiency at 200 °C of treated yam sunlight absorber was about 90%, and the evaporation rate of the water body reached 1.3164 kg m^{-2} h^{-1}. The conversion efficiencies of absorbers under different suns were different, under 3 sun illumination, the conversion efficiency was about 60%, and the evaporation rate of water body was the largest at 2.6838 kg m^{-2} h^{-1}. Under the same conditions, the solar-water vapor conversion efficiencies of the experimentally prepared bilayer yam solar absorbers were similar and both lower than those of the carbon-treated absorbers. The preparation process of the treated yam absorber is simple and the raw materials are cheap, which is expected to be applied in practical production.

ACKNOWLEDGEMENTS

The authors are grateful to the National Natural Science Foundation of China (Grant No. 51962018, 52163028), Industrial Support Project of Education Department of Gansu Province (2021CYZC-10), Innovation and Entrepreneurship Talent Project of Lanzhou (Grant No. 2020-RC-2, 2019-RC-2).

DECLARATION OF COMPETING INTEREST

The authors declare that they have no known competing financial interests or personal relationships that could have appeared to influence the work reported in this paper.

DATA AVAILABILITY

Data will be made available on request.

REFERENCES

1. J. Xu, Z. Wang, C. Chang, C. Song, J. Wu, W. Shang, P. Tao and T. Deng, *ACS Omega*, **4**, 16603 (2019).
2. W. Gan, Y. Wang, S. Xiao, R. Gao, Y. Shang, Y. Xie, J. Liu and J. Li, *ACS Appl. Mater. Interfaces*, **13**, 7756 (2021).
3. D. N. Thoai, Q. T. Hoai Ta, T. T. Truong, H. Van Nam and G. Van Vo, *J. Clean. Prod.*, **293**, 126122 (2021).
4. L. Chen, P. Xu, K. Kota, S. Kuravi and H. Wang, *Chemosphere*, **269**, 129372 (2021).
5. T. Xu, Y. Xu, J. Wang, H. Lu, W. Liu and J. Wang, *Chem. Eng. J.*, **415**, 128893 (2021).
6. X. Wang, Q. Gan, R. Chen, H. Peng, T. Zhang and M. Ye, *ACS Sustain. Chem. Eng.*, **8**, 7753 (2020).
7. M. Gao, C. K. Peh, F. L. Meng and G. W. Ho, *Small Methods*, **5**, 1 (2021).
8. M. Gao, C. K. Peh, L. Zhu, G. Yilmaz and G. W. Ho, *Adv. Energy Mater.*, **10**, 1 (2020).
9. F. L. Meng, M. Gao, T. Ding, G. Yilmaz, W. L. Ong and G. W. Ho, *Adv. Funct. Mater.*, **30**, 1 (2020).
10. Z. Wang, X. Wu, F. He, S. Peng and Y. Li, *Adv. Funct. Mater.*, **31**, 1 (2021).
11. S. He, C. Chen, Y. Kuang, R. Mi, Y. Liu, Y. Pei, W. Kong, W. Gan, H. Xie, E. Hitz, C. Jia, X. Chen, A. Gong, J. Liao, J. Li, Z. J. Ren, B. Yang, S. Das and L. Hu, *Energy Environ. Sci.*, **12**, 1558 (2019).
12. F. Li, N. Li, S. Wang, L. Qiao, L. Yu, P. Murto and X. Xu, *Adv. Funct. Mater.*, **31**, 1 (2021).
13. Y. Shi, O. Ilic, H. A. Atwater and J. R. Greer, *Nat. Commun.*, **12**, 1 (2021).
14. A. Vyatskikh, A. Kudo, S. Delalande and J. R. Greer, *Mater. Today Commun.*, **15**, 288 (2018).
15. S. Meng, X. Zhao, C. Y. Tang, P. Yu, R. Y. Bao, Z. Y. Liu, M. B. Yang and W. Yang, *J. Mater. Chem. A*, **8**, 2701 (2020).
16. S. S. Das, V. M. Pedireddi, A. Bandopadhyay, P. Saha and S. Chakraborty, *Nano Lett.*, **19**, 7191 (2019).
17. J. Chen, B. Li, G. Hu, R. Aleisa, S. Lei, F. Yang, D. Liu, F. Lyu, M. Wang, X. Ge, F. Qian, Q. Zhang and Y. Yin, *Nano Lett.*, **20**, 6051 (2020).
18. X. Zhang, Y. Peng, L. Shi and R. Ran, *ACS Sustain. Chem. Eng.*, **8**, 18114 (2020).
19. Y. Zhou, T. Ding, M. Gao, K. H. Chan, Y. Cheng, J. He and G. W. Ho, *Nano Energy*, **77**, 105102 (2020).
20. W. Fang, L. Zhao, X. He, H. Chen, W. Li, X. Zeng, X. Chen, Y. Shen and W. Zhang, *Renew. Energy*, **151**, 1067 (2020).
21. L. Chen, M. Xia, J. Du, X. Luo, L. Zhang and A. Li, *ChemSusChem*, **13**, 493 (2020).
22. Y. Lu, X. Wang, D. Fan, H. Yang, H. Xu, H. Min and X. Yang, *Sustain. Mater. Technol.*, **25**, e00180 (2020).
23. C. Sheng, N. Yang, Y. Yan, X. Shen, C. Jin, Z. Wang and Q. Sun, *Appl. Therm. Eng.*, **167**, 114712 (2020).
24. L. Zhu, L. Sun, H. Zhang, D. Yu, H. Aslan, J. Zhao, Z. Li, M. Yu, F. Besenbacher and Y. Sun, *Nano Energy*, **57**, 842 (2019).
25. Y. Yang, X. Yang, L. Fu, M. Zou, A. Cao, Y. Du, Q. Yuan and C. H. Yan, *ACS Energy Lett.*, **3**, 1165 (2018).
26. J. Li, X. Wang, Z. Lin, N. Xu, X. Li, J. Liang, W. Zhao, R. Lin, B. Zhu, G. Liu, L. Zhou, S. Zhu and J. Zhu, *Joule*, **4**, 928 (2020).
27. E. Chiavazzo, M. Morciano, F. Viglino, M. Fasano and P. Asinari, *Nat. Sustain.*, **1**, 763 (2018).
28. H. Yao, P. Zhang, C. Yang, Q. Liao, X. Hao, Y. Huang, M. Zhang, X. Wang, T. Lin, H. Cheng, J. Yuan and L. Qu, *Energy Environ. Sci.*, **14**, 5330 (2021).
29. J. Jia, W. Liang, H. Sun, Z. Zhu, C. Wang and A. Li, *Chem. Eng. J.*, **361**, 999 (2019).
30. J. Yang, Y. Chen, X. Jia, Y. Li, S. Wang and H. Song, *ACS Appl.*

Mater. Interfaces, **12**, 47029 (2020).
31. H. Jiang, X. Geng, S. Li, H. Tu, J. Wang, L. Bao, P. Yang and Y. Wan, *J. Mater. Sci. Technol.*, **59**, 180 (2020).
32. N. Xu, X. Hu, W. Xu, X. Li, L. Zhou, S. Zhu and J. Zhu, *Adv. Mater.*, **29**, 1 (2017).
33. X. Wu, G. Y. Chen, W. Zhang, X. Liu and H. Xu, *Adv. Sustain. Syst.*, **1**, 1700046 (2017).
34. B. Liang, J. Lv, G. Wang and T. Noritatsu, *Pigment Resin Technol.*, **46**, 172 (2017).
35. C. Brett, *Natl. Sci. Rev.*, **8** (2021), doi:10.1093/nsr/nwab036.
36. M. Zhu, J. Yu, C. Ma, C. Zhang, D. Wu and H. Zhu, *Sol. Energy Mater. Sol. Cells*, **191**, 83 (2019).
37. Z. Zhang, P. Mu, J. He, Z. Zhu, H. Sun, H. Wei, W. Liang and A. Li, *ChemSusChem*, **12**, 426 (2019).
38. T. Y. Ma, S. Dai, M. Jaroniec and S. Z. Qiao, *Angew. Chemie - Int. Ed.*, **53**, 7281 (2014).
39. Y. Liu, H. Yang, Y. Wang, C. Ma, S. Luo, Z. Wu, Z. Zhang, W. Li and S. Liu, *Chem. Eng. J.*, **424**, 130426 (2021).
40. H. Zhang, Z. Liu, J. Mai, N. Wang, J. Zhong, X. Mai and N. Zhang, *Chem. Eng. J.*, **411**, 128482 (2021).
41. A. Wang Jr., *The effect of annealing and ultra-high-pressure treatment on structural and functional of three starches with different polymorphs*, Tianjin University pf Science and Technology (2016).